Machine-learned tuning of artificial Kitaev chains from tunneling spectroscopy measurements

Jacob Benestad [1,*] Athanasios Tsintzis [2] Rubén Seoane Souto [3,2] Martin Leijnse [2]
Evert van Nieuwenburg [4] and Jeroen Danon [1]

[1]*Center for Quantum Spintronics, Department of Physics, Norwegian University of Science and Technology, 7491 Trondheim, Norway*
[2]*Division of Solid State Physics and NanoLund, Lund University, S-22100 Lund, Sweden*
[3]*Instituto de Ciencia de Materiales de Madrid (ICMM), Consejo Superior de Investigaciones Científicas (CSIC), 28049 Madrid, Spain*
[4]*Lorentz Institute and Leiden Institute of Advanced Computer Science, Leiden University, P.O. Box 9506, 2300 RA Leiden, The Netherlands*

We demonstrate reliable machine-learned tuning of quantum-dot-based artificial Kitaev chains to Majorana sweet spots, using the covariance matrix adaptation algorithm. We show that a loss function based on local tunneling spectroscopy features of a chain with two additional sensor dots added at its ends provides a reliable metric to navigate parameter space and find points where crossed Andreev reflection and elastic cotunneling between neighboring sites balance in such a way to yield near-zero-energy modes with very high Majorana quality. We simulate tuning of two- and three-site Kitaev chains, where the loss function is found from calculating the low-energy spectrum of a model Hamiltonian that includes Coulomb interactions and finite Zeeman splitting. In both cases, the algorithm consistently converges towards high-quality sweet spots. Since tunneling spectroscopy provides one global metric for tuning all on-site potentials simultaneously, this presents a promising way towards tuning longer Kitaev chains, which are required for achieving topological protection of the Majorana modes.

I. INTRODUCTION

Realization and control of Majorana bound states (MBSs), which remain much sought after due to their nonlocal and topological nature, are a topic of intense study within condensed-matter physics [1–6]. The simple Kitaev model gives one example of a topological material where MBSs can be found [7], and recreating the ingredients of the Kitaev model with engineered hybrid devices is a very promising avenue in this pursuit [8]. While a lot of work has focused on making artificial chains using semiconductor nanowires proximitized by superconductors [9–16], device imperfections, such as material disorder, seem currently to be a major challenge for further progress in this direction [17–29].

An alternative is to rather use arrays of alternating normal and proximitized quantum dots to build an artificial Kitaev chain, which could circumvent some of the material disorder issues [30–37]. Signatures of so-called "Poor Man's Majoranas" (PMMs), which are nonlocal but lack topological protection, have been demonstrated in a two-site minimal artificial Kitaev chain [38–40]. An important challenge faced in this field is to make and tune devices that are long enough that they can host topologically protected Majoranas [30]. Recent progress along these lines includes control over three-site devices [41] and the observation of signatures of tuning to a Majorana sweet spot in three-site devices [42].

To tune these artificial Kitaev chains to a sweet spot, where an even-odd ground-state degeneracy coincides with maximal Majorana quality (which we will define later) of the part of the corresponding excitation that lives on the outer sites of the chain, it is necessary to tune the system parameters such that crossed Andreev reflection (CAR) and elastic cotunneling (ECT) processes via the proximitized dots are pairwise balanced in each link in the chain [43,44]. In experiment, one faces the challenge of imperfect information about said tuning parameters, due to microscopic details such as material imperfections and varying gate-lever arms. In practice, tuning has so far been done by working with pairs of sites at a time, since there are too many variables for navigating a global metric manually, where all dots are tuned simultaneously. Such sequential manual tuning across the chain can be time consuming, and at the same time one must be careful that the overall tuning remains correct each time a new pair is tuned [41,42]. Pairwise tuning becomes especially precarious for the case of strong tunnel couplings, where multidot renormalization effects can be expected. With single CAR and ECT processes thus depending on parameters all along the chain, it will be difficult to tune the system while only considering pairs of dots. Thus, tuning all dots simultaneously would be advantageous, and the fact that this would be very difficult for a human to do motivates us to investigate machine-learning methods to perform automated tuning.

Such automatic tuning has already been proposed as a way to mitigate disorder in bulk hybrid nanowire systems, by using an Aharonov-Bohm interferometer to get a metric of the Majorana quality that can be used as a global loss function [45]. A simpler and more practical probe of Majorana quality could be

---

*Contact author: jacob.d.benestad@ntnu.no

to perform a tunneling spectroscopy experiment while adding an extra sensor dot at the end of the system [9,46,47], which was recently investigated in the context of artificial Kitaev chains based on quantum-dot arrays [48]. Work has also been done on the machine-learned tuning of dot-based artificial Kitaev chains, in the context of using generative neural networks to automatically classify avoided crossings in charge-stability diagrams [49,50].

In this paper, we demonstrate automatic tuning in simulated two- and three-site artificial Kitaev chains using the covariance matrix adaptation evolutionary strategy (CMA-ES) [51–53] with tunneling spectroscopy through sensor dots at both ends of the chain as a metric to navigate parameter space. We first apply the tuning algorithm to a minimal (two-site) Kitaev chain, where locations of the sweet spots can be relatively easily determined by numerical calculations for a given set of tight-binding parameters [33], and we show how the algorithm indeed converges towards these points. We then consider a three-site chain (five physical dots), where the locations of the sweet spots are not known *a priori*. Also in this case, the algorithm converges to points with vanishing even-odd ground-state splitting and very high Majorana quality. We thus demonstrate the capability of the CMA-ES algorithm to navigate a large tuning parameter space and efficiently locate Majorana sweet spots, based on simple tunneling spectroscopy data.

The rest of this paper is structured as follows: In Sec. II we introduce the Hamiltonian for our quantum-dot-based artificial Kitaev model, and we explain the basic working of the CMA-ES algorithm used for the automatic tuning. In Sec. III we present our results for the automatic tuning, first for a two-site model in Sec. III A, and a three-site model in Sec. III B. Finally, we present a short conclusion in Sec. IV.

II. MODEL

We consider a similar setup to that presented in Refs. [34,48]: a linear array of quantum dots where every other dot is proximitized by a superconductor, and with the addition of extra sensor dots at each end of the chain. To make the optimization more robust, we probe the low-energy physics of the system first with the sensor dot added to the left side of the array and then a second time with the sensor dot on the right side. In an experiment, such freedom of changing sides for the sensor dot could be achieved by defining extra dots on both ends of the Kitaev chain and then "removing" the one that is not being used by lowering its outer barrier such that the dot becomes incorporated as a part of the lead.

We describe the full array of dots with the Hamiltonian

$$H^{(n,s)} = H^{(n)}_{\text{Kit}} + H^{(n,s)}_{\text{S}}, \qquad (1)$$

where $s = L, R$ indicates on which side the sensor dot is located and n labels the number of "Kitaev-chain" sites, i.e., the number of normal (nonproximitized) quantum dots.

The first term in Eq. (1) describes the Kitaev-chain part of the system, which includes normal dots and dots proximitized by a superconductor, together with spin-conserving and spin-

nonconserving hopping between them:

$$H^{(n)}_{\text{Kit}} = \sum_{j=1}^{n} \sum_{\sigma} \varepsilon_{j\sigma} d^{\dagger}_{j\sigma} d_{j\sigma} + \sum_{j=1}^{n} \frac{U}{2} n_j(n_j - 1) \qquad (2)$$

$$+ \sum_{j=1}^{n-1} [\varepsilon_{Sj} n_{Sj} + \Delta(d^{\dagger}_{Sj\uparrow} d^{\dagger}_{Sj\downarrow} + d_{Sj\downarrow} d_{Sj\uparrow})]$$

$$+ \sum_{j=1}^{n-1} \sum_{\sigma} \left[t_{j,Sj} d^{\dagger}_{j\sigma} d_{Sj\sigma} + t_{Sj,j+1} d^{\dagger}_{Sj\sigma} d_{(j+1)\sigma} \right.$$

$$\left. + \beta_{\sigma} (t^{\text{SO}}_{j,Sj} d^{\dagger}_{j\sigma} d_{Sj\bar{\sigma}} + t^{\text{SO}}_{Sj,j+1} d^{\dagger}_{Sj\sigma} d_{(j+1)\bar{\sigma}}) + \text{H.c.} \right],$$

where $d^{\dagger}_{j\sigma}$ ($d^{\dagger}_{Sj\sigma}$) is the creation operator for an electron with spin $\sigma = \uparrow, \downarrow$ on (proximitized) dot j (Sj), and $n_j = d^{\dagger}_{j\uparrow} d_{j\uparrow} + d^{\dagger}_{j\downarrow} d_{j\downarrow}$ ($n_{Sj} = d^{\dagger}_{Sj\uparrow} d_{Sj\uparrow} + d^{\dagger}_{Sj\downarrow} d_{Sj\downarrow}$) is the number operator on that dot. The normal dots are described by the first line in Eq. (2). Their on-site single-particle energy $\varepsilon_{j\sigma} = \varepsilon_j + E_Z \delta_{\sigma,\downarrow}$ is spin dependent, where E_Z is the Zeeman energy and ε_j can be tuned by nearby electrostatic gates V_j, and the charging energy associated with a doubly occupied normal dot is given by U. The second line in Eq. (2) describes the proximitized dots, labeled Sj. The proximity of the superconductor is expected to result in a strong reduction of the effective on-site g factors, which we incorporate by using spin-independent potentials ε_{Sj}, for simplicity. The superconductor will also efficiently screen the on-site Coulomb interactions on these dots, which we thus neglect here [54]. The proximity-induced pairing potential Δ is assumed to be real and equal for all proximitized dots. Finally, the last two lines in Eq. (2) describe the coupling between the dots. The parameters $t_{i,j}$ ($t^{\text{SO}}_{i,j}$) set the amplitude of spin-conserving (spin-nonconserving) hopping between dots i and j, where $\beta_{\uparrow,\downarrow} = \pm 1$.

The second term in Eq. (1) describes the sensor dots and hopping between the sensors and the Kitaev chain:

$$H^{(n,s)}_{\text{S}} = \sum_{\sigma} \varepsilon_{s\sigma} d^{\dagger}_{s\sigma} d_{s\sigma} + \frac{U}{2} n_s(n_s - 1)$$

$$+ \delta_{s,L} \sum_{\sigma} \left[t_{L,1} d^{\dagger}_{L\sigma} d_{1\sigma} + \beta_{\sigma} t^{\text{SO}}_{L,1} d^{\dagger}_{L\sigma} d_{1\bar{\sigma}} + \text{H.c.} \right]$$

$$+ \delta_{s,R} \sum_{\sigma} \left[t_{n,R} d^{\dagger}_{n\sigma} d_{R\sigma} + \beta_{\sigma} t^{\text{SO}}_{n,R} d^{\dagger}_{n\sigma} d_{R\bar{\sigma}} + \text{H.c.} \right],$$

$$(3)$$

using similar notation as above. In this case, $\varepsilon_{s\sigma} = \varepsilon_s + E_Z \delta_{\sigma,\downarrow}$ while the Kronecker delta functions $\delta_{s,L}$ and $\delta_{s,R}$ choose which sensor dot is included.

In the following, we will limit ourselves to the cases where the number of sites is either $n = 2$ or $n = 3$, which corresponds to chains of three and five physical dots, respectively. For the case with $n = 2$, locations of the sweet spots are known for the model we use [33] and we can thus use this case as a test bed to assess the basic working of the tuning algorithm. For the case with $n = 3$, we expect a larger number of sweet spots, the locations of which are not known *a priori*. This case will be used to investigate the robustness of the algorithm when operating in a higher-dimensional parameter space.
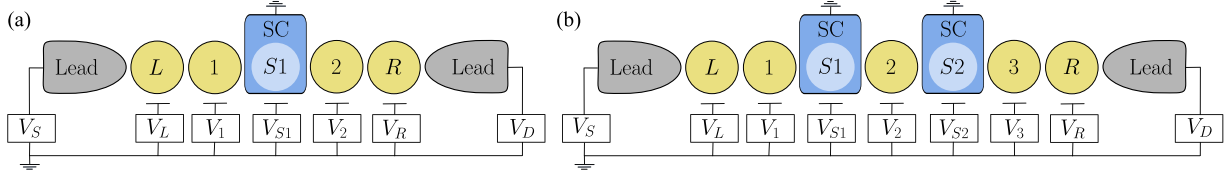
FIG. 1. Sketch of the artificial Kitaev chain systems considered in this paper. In addition to the sensor dots marked L/R on either side of the Kitaev chain, the array consists of (a) 3 dots or (b) 5 dots, where every other dot is proximitized by a superconductor (blue square) to create an Andreev bound state that can mediate CAR and ECT processes between the normal dots.

In an experiment, one would connect the chain to a source and drain lead (also indicated in Fig. 1) and measure the differential conductance across the array of dots as a function of ε_L or ε_R and the bias voltage applied to the source and drain. The location of the lowest-bias conductance peak then reveals the energy splitting between the lowest even and odd parity states of the array, and its dependence on the sensor-dot potential contains information about the Majorana quality of the states on the outer sites of the Kitaev chain [46–48]. The deviation from the ideal case (zero splitting independent of ε_L or ε_R) can then be quantified into a loss function used by the tuning algorithm to navigate parameter space, as we will detail in Sec. III. In our numerical simulations, it suffices to diagonalize $H^{(n,s)}$ and extract the even-odd ground-state splitting directly from its eigenenergies as this corresponds to the location of the lowest-bias peak [48], which saves considerable computational overhead as compared to simulating a full differential-conductance measurement.

To find the optimal set of tuning parameters $\varepsilon_{j,Sj}$ we use the CMA-ES algorithm [55], which is a simple evolution-strategy optimization technique, relying on stochastic sampling rather than derivatives, making it suitable for problems where the objective function to be minimized for instance has several local minima or is nonsmooth [51–53]. In our case, the limitation in sharpness of the conductance curves in real tunneling spectroscopy measurements due to broadening from temperature and tunnel coupling to the leads [56] was what motivated us to use a stochastic and derivative-free method: we can expect the limited resolution of an actual experiment to make it difficult to accurately evaluate derivatives of the loss function, likely rendering derivative-based unsuitable for optimization of the loss. Additionally, we are dealing with metrics containing several minima, where a purely derivative-based method may get lost in a nonoptimal local minimum.

The CMA-ES algorithm performs the optimization by iterative sampling from and updating of a multivariate normal (MvN) distribution. For each generation g, a number of $\lambda \geqslant 2$ offspring $\boldsymbol{\varepsilon}^{(g)}$, which in this case are configurations of the gate voltages to tune, are randomly drawn from a MvN distribution with mean $\boldsymbol{\mu}^{(g)}$ and covariance matrix $\Sigma^{(g)} = (\sigma^{(g)})^2 C^{(g)}$. The configurations $\boldsymbol{\varepsilon}^{(g)}$ and means $\boldsymbol{\mu}^{(g)}$ are thus $(2n-1)$-dimensional vectors, e.g., for the two-site Kitaev chain $\boldsymbol{\varepsilon}^{(g)} = \{\varepsilon_1^{(g)}, \varepsilon_{S1}^{(g)}, \varepsilon_2^{(g)}\}$. The offspring are then ranked according to their "fitness" using an objective (loss) function $\mathcal{L}(\boldsymbol{\varepsilon}^{(g)})$, and the MvN distribution is updated by calculating a new position $\boldsymbol{\mu}^{(g+1)}$, "stepsize" $(\sigma^{(g+1)})^2$, and "search direction" $C^{(g+1)}$, based on the η best-ranked offspring and the previous history

of changes to the population. A diagram of the CMA-ES optimization loop is shown in Fig. 2. We will consistently use $\lambda = 56$ and $\eta = 28$, based mainly on the computational resources available, and set all other fine-tuning parameters of the algorithm to the standard recommended values [51]. Specifically, the algorithm achieves convergence if (i) the range of best loss values across the last $10 + \lceil 30(2n-1)/\lambda \rceil$ generations or the range of all loss values in the last generation is smaller than 10^{-12} or (ii) if the standard deviation of all tuning parameters $\varepsilon_{j,Sj}$ becomes smaller than $10^{-12}\sigma^{(0)}$ [51]. We also terminate the algorithm if it exceeds 200 generations.
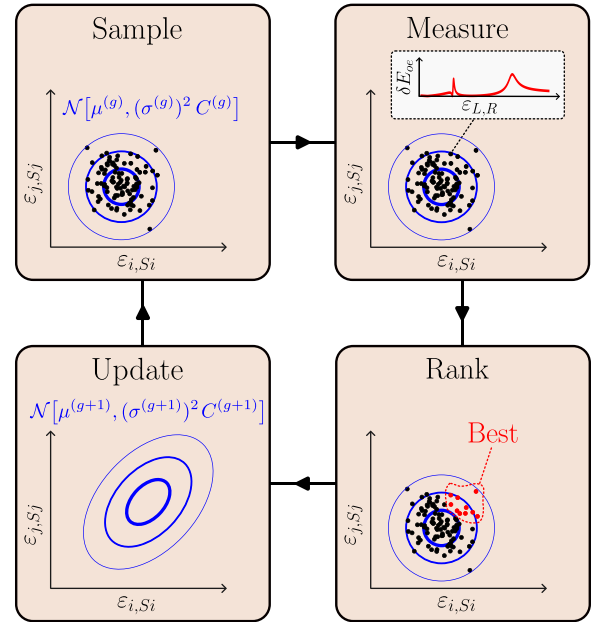

FIG. 2. Diagram of the CMA-ES algorithm interfaced to either a simulation or an actual experiment where local differential conductances are measured. Each generation can be divided into four stages: The first stage is to sample λ realizations from the MvN distribution to generate parameter configurations. In the second stage, each of these configurations is used in an experiment, where the dependence of the location of the low-bias conductance peaks (or the numerically determined lowest even-odd splittings) on the sensor-dot voltage provides a measure for the population fitness. The third stage is to rank all the parameter configurations according to this fitness. In the fourth stage, the MvN mean value and covariance matrix are updated based on a subset of the η best-ranked candidates.

III. RESULTS

For the tuning of an artificial Kitaev chain, it has been suggested that tracking the splitting between the lowest conductance peaks while sweeping the sensor-dot level ε_s can provide a metric for the Majorana quality [48]. Following this idea, we will investigate the performance of the CMA-ES algorithm using the loss function

$$f(\boldsymbol{\varepsilon}^{(g)}) = \frac{1}{2} \sum_{s=L,R} \max_{\varepsilon_s} \left| \frac{E_{0,n,s}^{\text{odd}} - E_{0,n,s}^{\text{even}}}{\Delta} \right|, \qquad (4)$$

where $E_{0,n,s}^{\text{odd}}$ and $E_{0,n,s}^{\text{even}}$ are the lowest eigenenergies of $H^{(n,s)}$, with total odd and even number of electrons, respectively. The loss function $f(\boldsymbol{\varepsilon}^{(g)})$ thus returns the maximum of the absolute energy splitting between the even and odd ground states over a sweep of the sensor-dot potential, averaged over the cases where the sensor dot is attached to the left or right side of the chain. The sweep range used for ε_s should cover both spin-species resonances, the locations of which could, e.g., be found roughly from estimates of E_Z, U, and Δ [46].

In addition, we make use of an L_2 regularization to penalize on-site potentials that grow large, as the amplitudes of CAR and ECT are inversely proportional to the energy difference between the bound states on neighboring dots [43], and the magnitude of these amplitudes ultimately sets the scale of the topological gap in longer chains. Combining L_2 regularization with the objective function Eq. (4), the final loss function we use to rank candidate parameter configurations is

$$\mathcal{L}(\boldsymbol{\varepsilon}^{(g)}) = f(\boldsymbol{\varepsilon}^{(g)}) + \alpha \left\| \frac{\boldsymbol{\varepsilon}^{(g)}}{\Delta} \right\|_2, \qquad (5)$$

where α parameterizes the L_2 regularization. For such regularization, one needs to establish some "origin" in parameter space, to determine $\|\boldsymbol{\varepsilon}^{(g)}\|_2$. Identifying in an experiment the true origin where $\boldsymbol{\varepsilon}^{(g)} = 0$ can be challenging, but small deviations from this point are not expected to pose an immediate problem as long as the origin used is not too far away from high-quality sweet spots.

Throughout, we will set all tunneling amplitudes to $t_{i,j} = 0.5\,\Delta$ and $t_{i,j}^{\text{SO}} = 0.1\,\Delta$, except for the ones describing the coupling to the sensor dot, where we use $t_{L,1} = t_{n,R} = 0.25\,\Delta$ and $t_{L,1}^{\text{SO}} = t_{n,R}^{\text{SO}} = 0.05\,\Delta$. The Zeeman energy is set to $E_Z = 1.5\,\Delta$ and the on-site Coulomb interaction strength for the normal dots to $U = 5\,\Delta$. These values are on purpose chosen the same as in Refs. [33,48], allowing for a straightforward comparison of the results. The mean of the initial distribution for the CMA-ES algorithm is always set to the origin, with an initial covariance matrix of $C^{(0)} = \mathbb{I}$, and $\sigma^{(0)} = 0.5\,\Delta$.

In all instances, we let the algorithm search for the optimal set of tuning parameters until it converges, using the loss function given in Eq. (5). We then assess the resulting set of tuning parameters $\boldsymbol{\varepsilon}^{\text{fin}}$ by evaluating (i) the resulting even-odd ground-state splitting in the Kitaev chain (without any sensor dot attached) $\delta E_{eo} = |E_{0,n}^{\text{odd}} - E_{0,n}^{\text{even}}|$, as well as (ii) the Majorana polarization (MP), given by [34,57–59]

$$M_j = \frac{\sum_\sigma \left(w_{j\sigma}^2 - z_{j\sigma}^2 \right)}{\sum_\sigma \left(w_{j\sigma}^2 + z_{j\sigma}^2 \right)}, \qquad (6)$$

where

$$w_{j\sigma} = \langle O | \, d_{j\sigma} + d_{j\sigma}^\dagger \, | E \rangle, \qquad (7)$$

$$z_{j\sigma} = \langle O | \, d_{j\sigma} - d_{j\sigma}^\dagger \, | E \rangle, \qquad (8)$$

where $|E\rangle$ and $|O\rangle$ are the even and odd ground states of $H_{\text{Kit}}^{(n)}$, respectively, and $E_{0,n}^{\text{even}}$ and $E_{0,n}^{\text{odd}}$ the corresponding ground-state energies. With this definition $-1 \leqslant M_j \leqslant 1$, and $|M_j| = 1$ corresponds to having a well-behaved single Majorana mode localized at site j. In Kitaev chains with finite Zeeman energy and Coulomb interactions, there exist in general no points in parameter space that have $\delta E_{eo} = 0$ and $|M_1| = |M_n| = 1$, which would indicate the existence of two "perfect" PMMs occupying the outer dots of the chain. Instead, it is common to look for sweet spots that maximize $|M_{1,n}|$ on the manifold in parameter space where $\delta E_{eo} = 0$ [33,34]. Below we will thus use δE_{eo} and the average MP $M \equiv (|M_1| + |M_n|)/2$ as measures for the success of the tuning procedure. Details of the CMA-ES workflow can be found in the Supplemental Material [60].

A. Two-site Kitaev chain

As a first benchmark, we test the optimization routine on a simulated minimal (two-site) Kitaev chain with $n = 2$ depicted in Fig. 1(a), where the sweet spots for our set of system parameters have been numerically calculated before [33], to see if it can reproduce the same results.

In Figs. 3(a) and 3(b) we show the even-odd ground-state splitting δE_{eo} and average polarization M as a function of $\varepsilon_{1,2}$ and ε_{S1}, calculated numerically from $H_{\text{Kit}}^{(2)}$. As expected, these plots are identical to the ones presented in Ref. [33], since we use the same model and same parameters. The two sweet spots identified in Ref. [33] are indicated with the two stars, and have $\delta E_{eo} = 0$ and $M = 0.986$.

Figures 3(c) and 3(d) display the first 60 generations of two example runs out of, in total, 50 simulations for the CMA-ES optimization algorithm, using the loss function given in Eq. (5) while setting $\alpha = 0$. In the case of the minimal Kitaev chain, the objective function landscape is simple enough that L_2 regularization is unnecessary; including a finite α would increase the probability for the algorithm to discover the left sweet spot, as the right sweet spot is further away from the origin $\boldsymbol{\varepsilon} = 0$ and therefore receives a larger punishment from the regularization. The solid lines in Figs. 3(c) and 3(d) show the evolution of the population mean of the three parameters and the shaded regions represent their marginal standard deviation. We see that from generation to generation the standard deviations of the population decrease, eventually vanishing as the mean value approaches a minimum in the loss.

Figure 3(c) shows a case where the algorithm converged towards the left sweet spot shown in Figs. 3(a) and 3(b), settling at the parameter configuration $\varepsilon_1 = \varepsilon_2 = -0.171\,\Delta$ and $\varepsilon_{S1} = -0.321\,\Delta$. The "target" values, corresponding to the corresponding sweet spot identified in Ref. [33], are indicated at the right vertical axis, where $\varepsilon_1^* = \varepsilon_2^* = -0.151\,\Delta$ and $\varepsilon_{S1}^* = -0.319\,\Delta$. In 41 cases out of 50, the algorithm converged towards this sweet spot. In the remaining 9 cases, the algorithm converged towards the other sweet spot, an example of which is shown in Fig. 3(d). Here, the final tuning parameters are $\varepsilon_1 = \varepsilon_2 = 0.0622\,\Delta$ and $\varepsilon_{S1} = 0.615\,\Delta$,
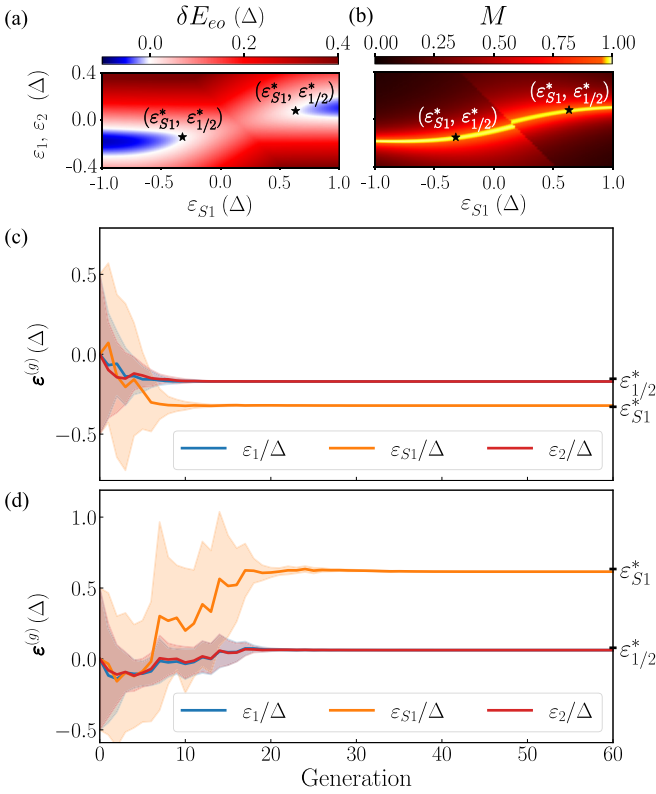
FIG. 3. (a) The difference between even and odd ground state energy of the two-site Kitaev chain without a sensor dot attached and (b) the average Majorana polarization at its outer sites as a function of $\varepsilon_{1,2}$ and ε_{S1}, cf. Ref. [33]. There are two sweet spots within the given parameter range, indicated by the black stars. (c),(d) The 60 first generations for two example runs of the CMA-ES algorithm for (c) a case that converged to the left sweet spot shown in (a),(b) and (d) a case that found the right sweet spot. Solid lines show the population mean of the parameters and the shaded regions give their marginal standard deviation.

which is again close to the true location of the right sweet spot at $\varepsilon_1^* = \varepsilon_2^* = 0.0785\,\Delta$ and $\varepsilon_{S1}^* = 0.634\,\Delta$. The bias towards finding the left sweet spot is due to the initial MvN being centered around $\varepsilon = 0$, which is closer to the left sweet spot than the right one. Convergence in these simulations was typically achieved after 80–100 generations.

Thus we see that the algorithm always converges to tuning parameters that indeed lie very close to the sweet spots found in Ref. [33], deviating from the sweet spots by Euclidian distances $\|\varepsilon - \varepsilon^*\|_2$ of $0.028\,\Delta$ and $0.030\,\Delta$ for the left and right sweet spots, respectively. As a result, the left sweet spot estimate found by the algorithm has $\delta E_{eo} = 2.7 \times 10^{-3}\,\Delta$ and $M = 0.967$ while the right sweet spot estimate has $\delta E_{eo} = 5.7 \times 10^{-3}\,\Delta$ and $M = 0.977$. In both cases we thus find high values for the MP and low splittings δE_{eo} [61], and the two-site Kitaev chain results indicate that the very simple tunneling spectroscopy metric together with the CMA-ES algorithm can indeed tune on-site potentials ε to their sweet spots.

B. Three-site Kitaev chain

To get an idea of how the automatic tuning will fare for longer chains, where the existence and locations of sweet
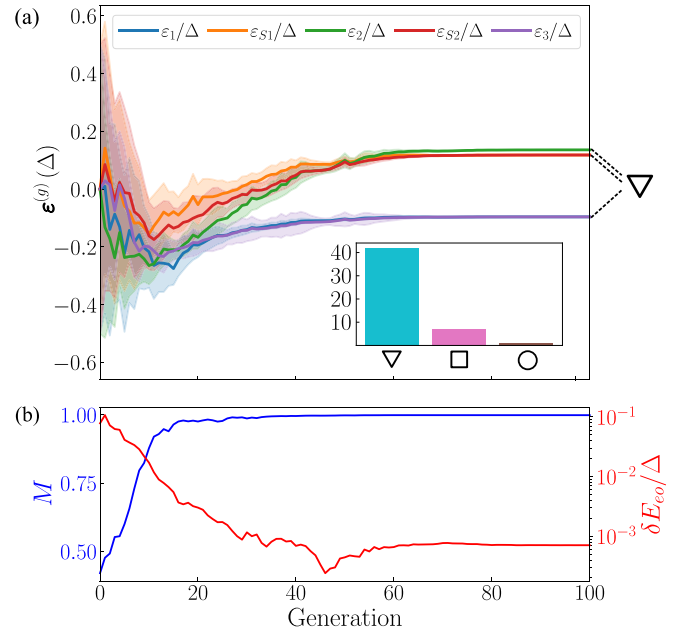

FIG. 4. Development of the 100 first generations for an example run of the CMA-ES algorithm for the three-site Kitaev chain, where it converges to the most commonly found parameter configuration. (a) Population mean of the parameters (solid lines) and their marginal standard deviation (shaded regions). (b) Majorana polarization M (blue) and even-odd ground-state splitting in the Kitaev chain δE_{oe} (red) for each of the first 100 generations. [Inset in (a)] Histogram of the occurrences of the three different sweet spots discovered in 50 simulations.

spots are not known, we also tested it for the case of $n = 3$, i.e., a five-dot array with two sensors as depicted in Fig. 1(b) corresponding to a three-site Kitaev chain. We again run the optimization 50 times, to obtain statistics on what solutions the algorithm tends to find. In this case we add an L_2 term with $\alpha = 0.02$ as described by Eq. (5). The larger α is set, the more biased the algorithm is towards finding the sweet spot that is closest to the origin $\varepsilon = 0$. In an experiment, this parameter should be tuned empirically, where in order to determine a suitable α one could run the algorithm first without any regularization to find the typical order of magnitude for the objective function, and based on this, one can estimate how much regularization is needed to keep the gate voltages inside a given parameter range.

The resulting automatically tuned potential configurations are summarized in Table I and a histogram of their occurrences is shown in the inset in Fig. 4(a). All of the simulations converge to configurations with MPs over 0.95 and even-odd splittings below $10^{-3}\,\Delta$. The exact sweet spot locations should have exactly zero δE_{eo}, and while we do see some finite value for all solutions, their small magnitude indicates that we get very close to the sweet spots. We see that a large majority of the runs (42 out of 50) ends up at a sweet spot with a MP of 0.998, which is significantly larger than at the two-site sweet spot. Indeed, the addition of extra sites is expected to increase the maximal MPs that can be achieved, as compared to the minimal two-site chain. To illustrate the working of the algorithm, we show the optimization process for one of

TABLE I. (left) Overview of the three configurations of automatically tuned on-site potentials found in 50 simulated experiments on a three-site Kitaev chain, using the loss function Eq. (5) with $\alpha = 0.02$. (right) The corresponding Majorana polarization, even-odd ground-state energy splitting, and final loss. The number of occurrences of each configuration is shown in the inset of Fig. 4(a).

	ε_1/Δ	ε_{S_1}/Δ	ε_2/Δ	ε_{S_2}/Δ	ε_3/Δ	MP	$\delta E_{eo}/\Delta$	Loss
$\triangledown$	-0.10	0.12	0.14	0.12	-0.10	0.998	7.1×10^{-4}	4.1×10^{-3}
$\square$	0.19	0.14	-0.31	-0.28	-0.18	0.979	2.5×10^{-4}	1.1×10^{-2}
$\bigcirc$	0.07	0.20	-0.40	-0.32	-0.18	0.985	8.7×10^{-4}	1.2×10^{-2}

these 42 high-MP simulations in Fig. 4. In Fig. 4(a) we show the CMA-ES population means and standard deviations for each parameter across generations and in Fig. 4(b) we plot the corresponding values for the MP M and energy splitting δE_{eo}.

We further note that for the 8 remaining cases the algorithm tuned the system to nonsymmetric parameter configurations with high MP and low δE_{eo}, see Table I, which looks odd at first sight. However, a feature of the three-site chain is that two pairs of ECT and CAR processes must be balanced rather than just one as in the minimal chain case. The balanced pairs may differ from each other, allowing indeed for nonsymmetrical configurations of the tuned on-site potentials along the chain. In principle, these nonsymmetric configurations could thus also correspond to valid sweet spots.

In the three-site chain simulations, convergence was achieved almost always within 140–200 generations due to the change in the loss function becoming smaller than the set tolerance, two exceptions being experiments that terminated as a result of reaching the 200-generation limit. We finally note that, as one increases the system size to longer and longer chains (without drastically increasing λ), it can be expected that the algorithm will to a lesser extent find one sweet spot most of the time, and rather discover several different minima. This is a result of the sample statistics becoming more and more sparse as the dimensionality of the parameter space becomes large. In the opposite limit (small dimensionality and many samples λ), we expect the algorithm to become more and more deterministic, approaching a situation where one is essentially checking all solutions within the search area given by the MvN.

IV. CONCLUSIONS

We have simulated short artificial Kitaev chains based on arrays of quantum dots, through exact diagonalization of a simple model Hamiltonian, and we showed that tunneling spectroscopy in the presence of additional sensor dots at the ends of the chain could be used to automatically tune the system to a Majorana sweet spot, for which we specifically used the CMA-ES algorithm in this work. We tested a simple metric based solely on the maximum difference between even and odd ground-state energies as a function of the sensor-dot voltages, suggested by Ref. [48], together with L_2 regularization on the gate voltages. For a two-site chain, the algorithm was able to find the known sweet spots for this system, as identified in Ref. [33]. In the case of a three-site chain, the algorithm was also capable of reliably tuning to apparent sweet spots, provided sufficient L_2 regularization was applied. We conclude that a simultaneous automatic tuning of all on-site potentials using tunneling spectroscopy through sensor dots and the CMA-ES algorithm presents a promising way forward for automatizing the search for Majorana sweet spots in quantum-dot-based artificial Kitaev chains.

[1] C. W. J. Beenakker, Search for Majorana fermions in superconductors, Annu. Rev. Condens. Matter Phys. **4**, 113 (2013).

[2] C. W. J. Beenakker, Search for non-Abelian Majorana braiding statistics in superconductors, SciPost Phys. Lect. Notes, 15 (2020).

[3] D. Aasen, M. Hell, R. V. Mishmash, A. Higginbotham, J. Danon, M. Leijnse, T. S. Jespersen, J. A. Folk, C. M. Marcus, K. Flensberg, and J. Alicea, Milestones toward Majorana-based quantum computing, Phys. Rev. X **6**, 031016 (2016).

[4] J. Alicea, New directions in the pursuit of Majorana fermions in solid state systems, Rep. Prog. Phys. **75**, 076501 (2012).

[5] J. Alicea, Y. Oreg, G. Refael, F. von Oppen, and M. P. A. Fisher, Non-Abelian statistics and topological quantum information processing in 1D wire networks, Nat. Phys. **7**, 412 (2011).

[6] C. Nayak, S. H. Simon, A. Stern, M. Freedman, and S. Das Sarma, Non-Abelian anyons and topological quantum computation, Rev. Mod. Phys. **80**, 1083 (2008).

[7] A. Y. Kitaev, Unpaired Majorana fermions in quantum wires, Phys.-Usp. **44**, 131 (2001).

[8] K. Flensberg, F. von Oppen, and A. Stern, Engineered platforms for topological superconductivity and Majorana zero modes, Nat. Rev. Mater. **6**, 944 (2021).

[9] M. T. Deng, S. Vaitiekėnas, E. B. Hansen, J. Danon, M. Leijnse, K. Flensberg, J. Nygård, P. Krogstrup, and C. M. Marcus, Majorana bound state in a coupled quantum-dot hybrid-nanowire system, Science **354**, 1557 (2016).

[10] M. T. Deng, C. L. Yu, G. Y. Huang, M. Larsson, P. Caroff, and H. Q. Xu, Anomalous zero-bias conductance peak in a Nb–InSb nanowire–Nb hybrid device, Nano Lett. **12**, 6414 (2012).

[11] A. D. K. Finck, D. J. Van Harlingen, P. K. Mohseni, K. Jung, and X. Li, Anomalous modulation of a zero-bias peak in a hybrid nanowire-superconductor device, Phys. Rev. Lett. **110**, 126406 (2013).

[12] R. M. Lutchyn, J. D. Sau, and S. D. Sarma, Majorana fermions and a topological phase transition in semiconductor-superconductor heterostructures, Phys. Rev. Lett. **105**, 077001 (2010).

[13] V. Mourik, K. Zuo, S. M. Frolov, S. R. Plissard, E. P. A. M. Bakkers, and L. P. Kouwenhoven, Signatures of Majorana fermions in hybrid superconductor-semiconductor nanowire devices, Science **336**, 1003 (2012).

[14] F. Nichele, A. C. C. Drachmann, A. M. Whiticar, E. C. O'Farrell, H. J. Suominen, A. Fornieri, T. Wang, G. C. Gardner, C. Thomas, A. T. Hatke, P. Krogstrup, M. J. Manfra, K. Flensberg, and C. M. Marcus, Scaling of Majorana zero-bias conductance peaks, Phys. Rev. Lett. **119**, 136803 (2017).

[15] Y. Oreg, G. Refael, and F. von Oppen, Helical liquids and Majorana bound states in quantum wires, Phys. Rev. Lett. **105**, 177002 (2010).

[16] E. Prada, P. San-Jose, M. W. A. de Moor, A. Geresdi, E. J. H. Lee, J. Klinovaja, D. Loss, J. Nygård, R. Aguado, and L. P. Kouwenhoven, From Andreev to Majorana bound states in hybrid superconductor–semiconductor nanowires, Nat. Rev. Phys. **2**, 575 (2020).

[17] J. Liu, A. C. Potter, K. T. Law, and P. A. Lee, Zero-bias peaks in the tunneling conductance of spin-orbit-coupled superconducting wires with and without Majorana end-states, Phys. Rev. Lett. **109**, 267002 (2012).

[18] D. I. Pikulin, J. P. Dahlhaus, M. Wimmer, H. Schomerus, and C. W. J. Beenakker, A zero-voltage conductance peak from weak antilocalization in a Majorana nanowire, New J. Phys. **14**, 125011 (2012).

[19] G. Kells, D. Meidan, and P. W. Brouwer, Near-zero-energy end states in topologically trivial spin-orbit coupled superconducting nanowires with a smooth confinement, Phys. Rev. B **86**, 100503 (2012).

[20] H. Zhang, Ö. Gül, S. Conesa-Boj, M. P. Nowak, M. Wimmer, K. Zuo, V. Mourik, F. K. de Vries, J. van Veen, M. W. A. de Moor, J. D. S. Bommer, D. J. van Woerkom, D. Car, S. R. Plissard, E. P. A. M. Bakkers, M. Quintero-Pérez, M. C. Cassidy, S. Koelling, S. Goswami, K. Watanabe, T. Taniguchi, and L. P. Kouwenhoven, Ballistic superconductivity in semiconductor nanowires, Nat. Commun. **8**, 16025 (2017).

[21] C. Reeg, O. Dmytruk, D. Chevallier, D. Loss, and J. Klinovaja, Zero-energy Andreev bound states from quantum dots in proximitized Rashba nanowires, Phys. Rev. B **98**, 245407 (2018).

[22] B. D. Woods, J. Chen, S. M. Frolov, and T. D. Stanescu, Zero-energy pinning of topologically trivial bound states in multiband semiconductor-superconductor nanowires, Phys. Rev. B **100**, 125407 (2019).

[23] H. Pan and S. Das Sarma, Physical mechanisms for zero-bias conductance peaks in Majorana nanowires, Phys. Rev. Res. **2**, 013377 (2020).

[24] S. Ahn, H. Pan, B. Woods, T. D. Stanescu, and S. Das Sarma, Estimating disorder and its adverse effects in semiconductor Majorana nanowires, Phys. Rev. Mater. **5**, 124602 (2021).

[25] S. D. Sarma and H. Pan, Disorder-induced zero-bias peaks in Majorana nanowires, Phys. Rev. B **103**, 195158 (2021).

[26] P. Yu, J. Chen, M. Gomanko, G. Badawy, E. P. A. M. Bakkers, K. Zuo, V. Mourik, and S. M. Frolov, Non-Majorana states yield nearly quantized conductance in proximatized nanowires, Nat. Phys. **17**, 482 (2021).

[27] R. Hess, H. F. Legg, D. Loss, and J. Klinovaja, Local and nonlocal quantum transport due to Andreev bound states in finite Rashba nanowires with superconducting and normal sections, Phys. Rev. B **104**, 075405 (2021).

[28] J. Cayao and P. Burset, Confinement-induced zero-bias peaks in conventional superconductor hybrids, Phys. Rev. B **104**, 134507 (2021).

[29] R. Hess, H. F. Legg, D. Loss, and J. Klinovaja, Trivial Andreev band mimicking topological bulk gap reopening in the nonlocal conductance of long Rashba nanowires, Phys. Rev. Lett. **130**, 207001 (2023).

[30] J. D. Sau and S. D. Sarma, Realizing a robust practical Majorana chain in a quantum-dot-superconductor linear array, Nat. Commun. **3**, 964 (2012).

[31] M. Leijnse and K. Flensberg, Parity qubits and poor man's Majorana bound states in double quantum dots, Phys. Rev. B **86**, 134528 (2012).

[32] S. Miles, D. van Driel, M. Wimmer, and C.-X. Liu, Kitaev chain in an alternating quantum dot-Andreev bound state array, arXiv:2309.15777.

[33] A. Tsintzis, R. S. Souto, and M. Leijnse, Creating and detecting poor man's Majorana bound states in interacting quantum dots, Phys. Rev. B **106**, L201404 (2022).

[34] A. Tsintzis, R. S. Souto, K. Flensberg, J. Danon, and M. Leijnse, Majorana qubits and non-Abelian physics in quantum dot–based minimal Kitaev chains, PRX Quantum **5**, 010323 (2024).

[35] J. D. T. Luna, A. M. Bozkurt, M. Wimmer, and C.-X. Liu, Flux-tunable Kitaev chain in a quantum dot array, arXiv:2402.07575.

[36] C.-X. Liu, H. Pan, F. Setiawan, M. Wimmer, and J. D. Sau, Fusion protocol for Majorana modes in coupled quantum dots, Phys. Rev. B **108**, 085437 (2023).

[37] R. S. Souto and R. Aguado, Subgap states in semiconductor-superconductor devices for quantum technologies: Andreev qubits and minimal Majorana chains, arXiv:2404.06592.

[38] T. Dvir, G. Wang, N. van Loo, C.-X. Liu, G. P. Mazur, A. Bordin, S. L. D. ten Haaf, J.-Y. Wang, D. van Driel, F. Zatelli, X. Li, F. K. Malinowski, S. Gazibegovic, G. Badawy, E. P. A. M. Bakkers, M. Wimmer, and L. P. Kouwenhoven, Realization of a minimal Kitaev chain in coupled quantum dots, Nature (London) **614**, 445 (2023).

[39] S. L. D. ten Haaf, Q. Wang, A. M. Bozkurt, C.-X. Liu, I. Kulesh, P. Kim, D. Xiao, C. Thomas, M. J. Manfra, T. Dvir,

M. Wimmer, and S. Goswami, A two-site Kitaev chain in a two-dimensional electron gas, Nature **630**, 329 (2024).

[40] F. Zatelli, D. van Driel, D. Xu, G. Wang, C.-X. Liu, A. Bordin, B. Roovers, G. P. Mazur, N. van Loo, J. C. Wolff, A. M. Bozkurt, G. Badawy, S. Gazibegovic, E. P. A. M. Bakkers, M. Wimmer, L. P. Kouwenhoven, and T. Dvir, Robust poor man's Majorana zero modes using Yu-Shiba-Rusinov states, arXiv:2311.03193.

[41] A. Bordin, X. Li, D. van Driel, J. C. Wolff, Q. Wang, S. L. D. ten Haaf, G. Wang, N. van Loo, L. P. Kouwenhoven, and T. Dvir, Crossed Andreev reflection and elastic cotunneling in three quantum dots coupled by superconductors, Phys. Rev. Lett. **132**, 056602 (2024).

[42] A. Bordin, C.-X. Liu, T. Dvir, F. Zatelli, S. L. D. ten Haaf, D. van Driel, G. Wang, N. van Loo, T. van Caekenberghe, J. C. Wolff, Y. Zhang, G. Badawy, S. Gazibegovic, E. P. A. M. Bakkers, M. Wimmer, L. P. Kouwenhoven, and G. P. Mazur, Signatures of Majorana protection in a three-site Kitaev chain, arXiv:2402.19382.

[43] C.-X. Liu, G. Wang, T. Dvir, and M. Wimmer, Tunable superconducting coupling of quantum dots via Andreev bound states in semiconductor-superconductor nanowires, Phys. Rev. Lett. **129**, 267701 (2022).

[44] C.-X. Liu, A. M. Bozkurt, F. Zatelli, S. L. D. ten Haaf, T. Dvir, and M. Wimmer, Enhancing the excitation gap of a quantum-dot-based Kitaev chain, arXiv:2310.09106.

[45] M. Thamm and B. Rosenow, Machine learning optimization of Majorana hybrid nanowires, Phys. Rev. Lett. **130**, 116202 (2023).

[46] E. Prada, R. Aguado, and P. San-Jose, Measuring Majorana nonlocality and spin structure with a quantum dot, Phys. Rev. B **96**, 085418 (2017).

[47] D. J. Clarke, Experimentally accessible topological quality factor for wires with zero energy modes, Phys. Rev. B **96**, 201109 (2017).

[48] R. S. Souto, A. Tsintzis, M. Leijnse, and J. Danon, Probing Majorana localization in minimal Kitaev chains through a quantum dot, Phys. Rev. Res. **5**, 043182 (2023).

[49] R. Koch, D. van Driel, A. Bordin, J. L. Lado, and E. Greplova, Adversarial Hamiltonian learning of quantum dots in a minimal Kitaev chain, Phys. Rev. Appl. **20**, 044081 (2023).

[50] D. van Driel, R. Koch, V. P. M. Sietses, S. L. D. ten Haaf, C.-X. Liu, F. Zatelli, B. Roovers, A. Bordin, N. van Loo, G. Wang, J. C. Wolff, G. P. Mazur, T. Dvir, I. Kulesh, Q. Wang, A. M. Bozkurt, S. Gazibegovic, G. Badawy, E. P. A. M. Bakkers, M.

Wimmer, S. Goswami, J. L. Lado, L. P. Kouwenhoven, and E. Greplova, Cross-platform autonomous control of minimal Kitaev chains, arXiv:2405.04596.

[51] N. Hansen, The CMA evolution strategy: A tutorial, arXiv:1604.00772.

[52] N. Hansen and A. Ostermeier, Completely derandomized self-adaptation in evolution strategies, Evol. Comput. **9**, 159 (2001).

[53] N. Hansen, S. D. Müller, and P. Koumoutsakos, Reducing the time complexity of the derandomized evolution strategy with covariance matrix adaptation (CMA-ES), Evol. Comput. **11**, 1 (2003).

[54] Including small Coulomb interactions on the proximitized dots does not change the qualitative results [33].

[55] We use the cma Python library from pypi.org/project/cma.

[56] L. P. Kouwenhoven, C. M. Marcus, P. L. McEuen, S. Tarucha, R. M. Westervelt, and N. S. Wingreen, Electron transport in quantum dots, in *Mesoscopic Electron Transport*, edited by L. L. Sohn, L. P. Kouwenhoven, and G. Schön (Springer Netherlands, Dordrecht, 1997), pp. 105–214.

[57] N. Sedlmayr and C. Bena, Visualizing Majorana bound states in one and two dimensions using the generalized Majorana polarization, Phys. Rev. B **92**, 115115 (2015).

[58] D. Sticlet, C. Bena, and P. Simon, Spin and Majorana polarization in topological superconducting wires, Phys. Rev. Lett. **108**, 096802 (2012).

[59] S. V. Aksenov, A. O. Zlotnikov, and M. S. Shustin, Strong Coulomb interactions in the problem of Majorana modes in a wire of the nontrivial topological class BDI, Phys. Rev. B **101**, 125431 (2020).

[60] See Supplemental Material at http://link.aps.org/supplemental/10.1103/PhysRevB.110.075402 for how the CMA-ES algorithm fits into the artificial Kitaev chain autotuning workflow, in addition to showing the mathematical details behind how the CMA-ES algorithm works.

[61] Although such residual δE_{eo} would still translate into a relatively short upper-bound time scale for "Majorana manipulation," it lies well within the resolution of an actual tunnelling-spectroscopy experiment, likely making it impossible to resolve such small energy splitting anyway. Furthermore, the automated tuning found here could serve as the starting point for a finer search using other methods.

[62] M. Själander, M. Jahre, G. Tufte, and N. Reissmann, EPIC: An energy-efficient, high-performance GPGPU computing research infrastructure, arXiv:1912.05848.